


RESEARCH

Open Access



Selected commensals educate the intestinal vascular and immune system for immunocompetence

Rossana Romero^{1,2}, Agnieszka Zarzycka^{1,3}, Mathieu Preussner¹, Florence Fischer^{1,4}, Torsten Hain^{5,6}, Jan-Paul Herrmann⁵, Katrin Roth⁷, Corinna U. Keber⁸, Kushal Suryamohan⁹, Hartmann Raifer¹⁰, Maik Luu^{1,11}, Hanna Leister¹, Wilhelm Bertrams¹², Matthias Klein¹³, Hosam Shams-Eldin¹⁴, Ralf Jacob¹⁵, Hans-Joachim Mollenkopf¹⁶, Krishnaraj Rajalingam², Alexander Visekruna¹ and Ulrich Steinhoff^{1,17*} 

Abstract

Background: The intestinal microbiota fundamentally guides the development of a normal intestinal physiology, the education, and functioning of the mucosal immune system. The *Citrobacter rodentium*-carrier model in germ-free (GF) mice is suitable to study the influence of selected microbes on an otherwise blunted immune response in the absence of intestinal commensals.

Results: Here, we describe that colonization of adult carrier mice with 14 selected commensal microbes (OMM¹² + MC²) was sufficient to reestablish the host immune response to enteric pathogens; this conversion was facilitated by maturation and activation of the intestinal blood vessel system and the step- and timewise stimulation of innate and adaptive immunity. While the immature colon of *C. rodentium*-infected GF mice did not allow sufficient extravasation of neutrophils into the gut lumen, colonization with OMM¹² + MC² commensals initiated the expansion and activation of the visceral vascular system enabling granulocyte transmigration into the gut lumen for effective pathogen elimination.

Conclusions: Consortium modeling revealed that the addition of two facultative anaerobes to the OMM¹² community was essential to further progress the intestinal development. Moreover, this study demonstrates the therapeutic value of a defined consortium to promote intestinal maturation and immunity even in adult organisms.

Keywords: Microbial consortia, Commensal imprinting, Asymptomatic infection, Endothelial cells, Blood vessel development, Intestinal maturation, Genome-guided microbiota, Neutrophils, *C. rodentium*, Oligo-Mouse-Microbiota, Colonization resistance, Enteric pathogen

Introduction

After birth, mammals successively acquire microbes on their mucosal surfaces with the most numerous communities residing in the gut. These slowly developing microbial communities not only help to digest our food and produce important bioactive substances but are essential for the maturation of immune cells and organ structures [1]. While full maturation of the human intestinal microbiota requires several years depending on nutrition, social

*Correspondence: ulrich.steinhoff@staff.uni-marburg.de

¹⁷ Biomedical Research Center (BMFZ), Institute for Medical Microbiology and Hygiene, University of Marburg, Hans Meerwein Straße 2, 35043 Marburg, Germany

Full list of author information is available at the end of the article



© The Author(s) 2022. **Open Access** This article is licensed under a Creative Commons Attribution 4.0 International License, which permits use, sharing, adaptation, distribution and reproduction in any medium or format, as long as you give appropriate credit to the original author(s) and the source, provide a link to the Creative Commons licence, and indicate if changes were made. The images or other third party material in this article are included in the article's Creative Commons licence, unless indicated otherwise in a credit line to the material. If material is not included in the article's Creative Commons licence and your intended use is not permitted by statutory regulation or exceeds the permitted use, you will need to obtain permission directly from the copyright holder. To view a copy of this licence, visit <http://creativecommons.org/licenses/by/4.0/>. The Creative Commons Public Domain Dedication waiver (<http://creativecommons.org/publicdomain/zero/1.0/>) applies to the data made available in this article, unless otherwise stated in a credit line to the data.

contacts, and pets [2], microbial colonization between birth and weaning is essential for normal development and immune reactivity [3]. This period is called *window of opportunity*, as the cross talk between commensals and their host during this time has long-term consequences for a healthy or pathological immune reactivity [4]. In contrast to early life, our understanding as to what extent commensal bacteria may affect the morphology and immune function of an adult organism is still incomplete. To this end, GF animals provide an ideal analytical tool, as the lack of commensals has profound and lifelong effects on the structural and functional development of the mucosal immune system [5]. Although transfer of a normal intestinal microbiota has been shown to correct many developmental and immune-related cellular pathways in these mice [6, 7], the complexity and variability of the microbiota make it difficult to assess whether tissue- and immune-related transcriptional responses after conventionalization are similar to normally raised specific-pathogen-free (SPF) mice [8]. Therefore, understanding the impact of defined bacteria or limited microbial consortia on maturation and development of tissue structures and the immune system would be a big advantage for the targeted intervention of acute and persisting infections.

For several pathogens, an unknown fraction of infected individuals is able to spread the disease even though they are free of symptoms [9]. As asymptomatic carriers handicap the control of pathogen transmission and unaware antibiotic treatment favors the emergence of drug-resistant strains, investigation of possible causes for carrier development is of utmost importance [10, 11].

We here analyzed the carrier phenomenon by using GF mice infected with *C. rodentium*, a murine pathogen that belongs to the family of extracellular enteric pathogens related to human enteropathogenic (EPEC) and enterohemorrhagic (EHEC) *Escherichia coli* [12, 13]. While animals with a normal laboratory microbiota (SPF) eradicate the pathogen, *C. rodentium* downregulates its virulence factors [14] and persists lifelong asymptotically in GF mice which, similar to asymptomatic human carriers, are able to spread the infection.

As the constellation of intestinal microbes that make up an individual's microbiome is highly unique [15], subtractive manipulation of a complex microbiota is challenging compared to the additive strategy which can also be applied in GF animals. A recently described model microbiota (Oligo-Mouse-Microbiota, OMM¹²) [16] alone or together with rationally selected microbes was used for their potential to convert adult *C. rodentium*-carrier mice into responder animals. We provide evidence that colonization of adult GF mice with OMM¹² induces maturation of intestinal blood vessels

and activation of the immune system to support neutrophil migration to reach the intestinal lumen where *C. rodentium* resides. Enforcing OMM¹² with two rationally selected microbes (*E. coli* and *Citrobacter amalonaticus*, MC²) further enhanced intestinal development and provided GF mice colonization resistance and immunity against *C. rodentium* comparable to conventional mice.

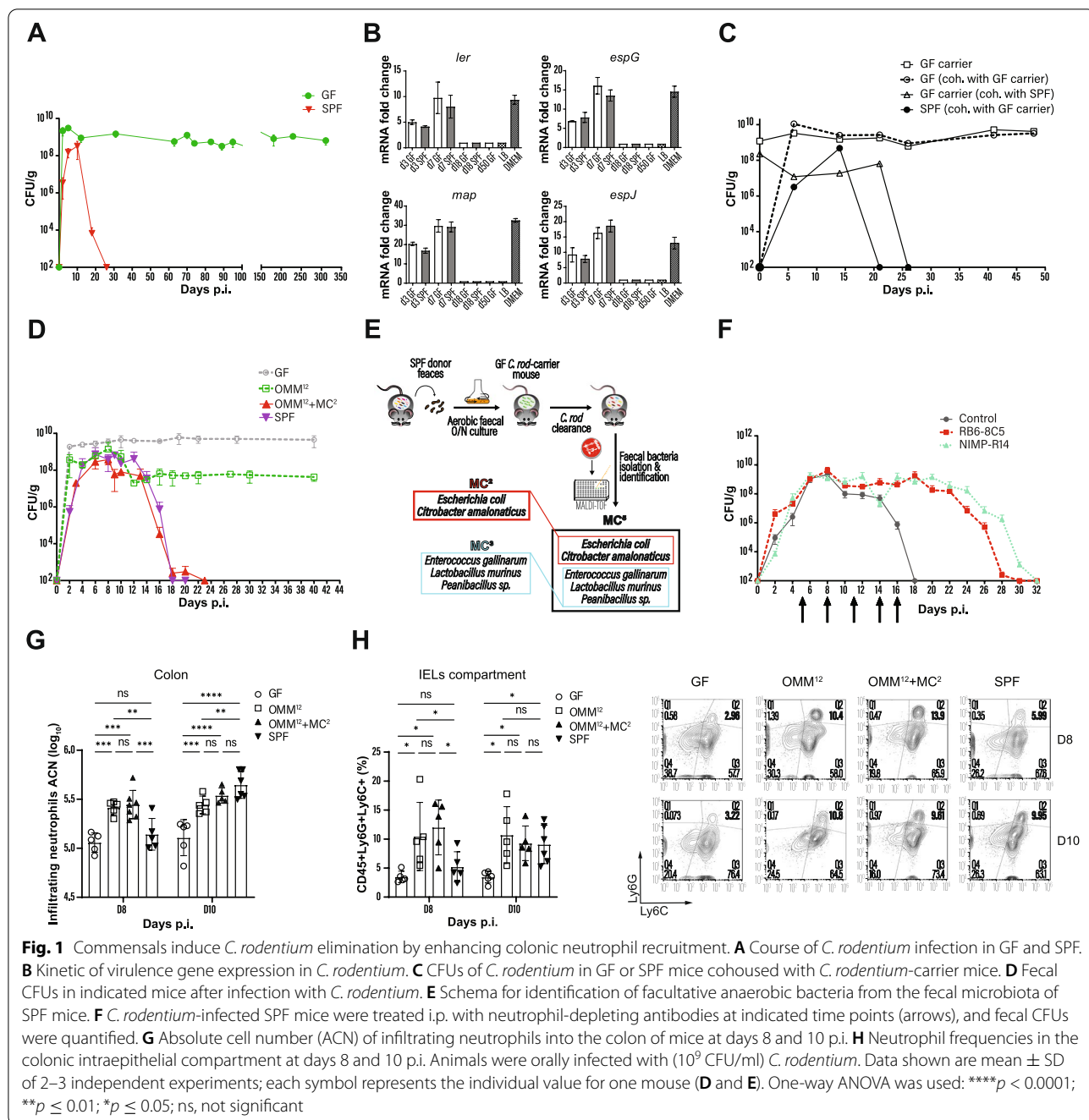
Thus, we hypothesized that the lack of defined intestinal microbes may contribute or favor the development of a pathogen carrier status which might be corrected by rational microbiota-based therapy.

Results

Fourteen commensals induce *C. rodentium* elimination by enhancing colonic neutrophil recruitment

Monitoring the infection of GF mice with *C. rodentium* for more than 1 year, we observed that animals devoid of microbiota turned into asymptomatic carriers, despite high bacterial loads (Fig. 1A). As recently described for EHEC and EPEC strains [17], the lack of *C. rodentium* pathogenicity was also associated with a downregulation of virulence genes, from day 18 p.i. (Fig. 1B), yet long-term persisting *C. rodentium* was still able to infect naïve mice (Fig. 1C).

Starting from the premise that conventionalization of GF mice triggers the elimination of *C. rodentium* (Fig. S1A), we searched for a defined bacterial community that confers colonization resistance and immunity in *C. rodentium* carriers by testing the OMM¹² microbiota model. OMM¹²-colonized mice infected with *C. rodentium* revealed that after the initial rapid multiplication, the pathogen load dropped markedly by day 10 and remained constant until the end of the experiment (Fig. 1D). Although OMM¹² caused a 200-fold pathogen reduction compared to GF mice, this consortium was not sufficient to mimic a complex microbiota (Fig. 1D). As facultative anaerobic bacteria are under-represented in the OMM¹² consortium, we mined the microbiota of SPF mice for strains that together with OMM¹² facilitate the clearance of *C. rodentium* in carrier mice as outlined in Fig. 1E. To lower the microbial complexity, feces from SPF mice were cultivated under aerobic conditions and transferred into *C. rodentium* carriers. As recipients of these fecal microbiota transplants (FMT) were able to eliminate the pathogen (Fig. S1B), we searched for commensals that were still present in these mice after pathogen elimination. A consortium of five facultative anaerobes was identified (MC⁵: *E. coli*, *C. amalonaticus*, *Enterococcus gallinarum*, *Lactobacillus murinus*, and *Paenibacillus* sp.) (Fig. 1E). Remarkably, enrichment of OMM¹² with MC⁵ (OMM¹² + MC⁵) was able to induce pathogen clearance (Fig. S1C). To further reduce the complexity, we selected *E. coli* and *C.*



amalonaticus (MC²), as both bacteria have been reported to induce colonization resistance against *C. rodentium* [14, 18]. OMM¹² mice associated with MC² prior to *C. rodentium* infection cleared the pathogen with kinetics similar to SPF and OMM¹² + MC⁵ mice (Figs. 1D and S1C). It should be noted that clearance of *C. rodentium* in OMM¹² + MC² mice was specifically promoted by MC² bacteria, as OMM¹² mice colonized with the remaining 3 facultative anaerobes from MC⁵, *E. gallinarum*, *L.*

murinus, and *Paenibacillus* sp. (MC³), failed to eliminate the infection, similar to OMM¹² mice (Fig. S1C).

Neutrophils are essential for the clearance of *C. rodentium* infection [19]. Accordingly, transient antibody-mediated depletion of neutrophils in SPF mice led to delayed pathogen clearance (Fig. 1F). Here, we examined the impact of the microbiota on neutrophil migration into the colon during the infection. *C. rodentium*-infected GF mice showed low neutrophil numbers in the colon that

peaked at day 8 p.i. and declined afterwards (Fig. S1D). SPF mice displayed a similar neutrophil migration pattern until day 8 p.i., followed by a sharp increase at day 10 p.i., a time point that coincides with the decline of *C. rodentium* titers in SPF mice (Fig. S1F and Fig. 1D). Since these findings suggest that migration of neutrophils into the colon is controlled by the intestinal microbiota rather than by the pathogen (Fig. 2), neutrophil numbers were examined in OMM¹² and OMM¹² + MC² mice. In comparison with GF, OMM¹² and OMM¹² + MC² mice showed significantly increased infiltrations of neutrophils on day 8 p.i. which was comparable to SPF mice on day 10 p.i. (Fig. 1G), demonstrating that OMM¹² colonization was sufficient to induce a robust migration of neutrophils into the colon on both days (Fig. 1G).

C. rodentium is an extracellular pathogen that adheres to the luminal site of the intestinal epithelium [20];

thus, neutrophils must migrate through the lamina propria (LP) and cross the epithelial barrier to reach the gut lumen for pathogen engulfment [19]. Therefore, we studied the influence of microbial consortia on neutrophil migration into the colonic LP and those migrating through the epithelial lining during infection. As previously reported for GF and SPF mice [14], the frequencies of LP neutrophils were also similar in OMM¹² and OMM¹² + MC² mice (Fig. S1E). Conversely, neutrophils isolated from the intraepithelial compartment were markedly reduced in GF mice on days 8 and 10 p.i. compared to OMM¹², OMM¹² + MC², and SPF mice (Fig. 1H). Notably, the varying numbers of intestinal neutrophils were not related to differences in numbers of blood neutrophils, as these were independent of the intestinal microbiota (Fig. S1F). Collectively, these data suggest a microbiota-triggered mechanism for neutrophil

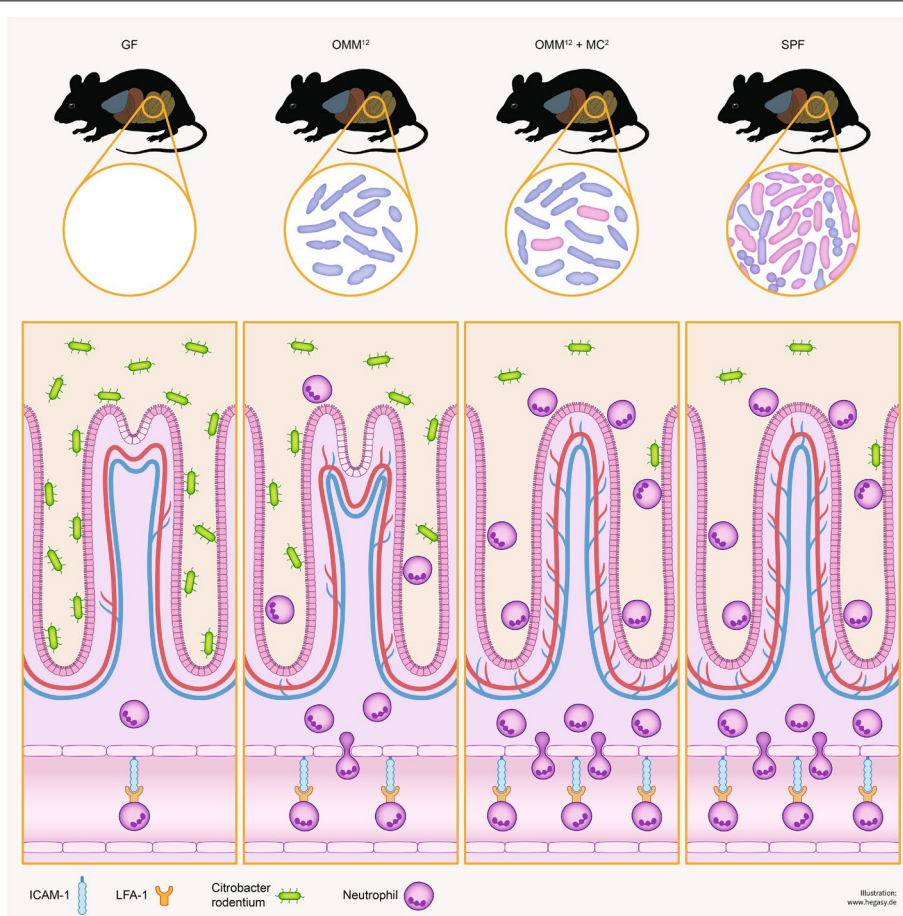


Fig. 2 Influence of commensals on maturation of the vascular and immune system. Sketch shows crypts, blood vessels, *C. rodentium* and neutrophils under different colonization conditions. GF mice have an immature colon and when infected with *C. rodentium*, they become lifelong carriers with high pathogen titers and low numbers of neutrophils in the colon. Colonization of GF animals with the OMM¹² microbiota prior to *C. rodentium* infection leads to partial maturation of the colonic blood vessels and crypts. Furthermore, OMM¹² colonization activates endothelial cells allowing neutrophils to extravasate into the lamina propria and lumen of the colon, with partial elimination of *C. rodentium*. Addition of MC² to the OMM¹² consortium further enhances tissue maturation of the colon allowing clearance of *C. rodentium* comparable to SPF mice

recruitment into the colonic lumen during *C. rodentium* infection.

Commensals activate the intestinal endothelium

Extravasation of neutrophils requires the expression of LFA-1 on their surface and its interaction with ICAM-1 on endothelial cells for neutrophil arrest and diapedesis [21, 22]. During *C. rodentium* infection, high expression of LFA-1 was observed on blood and colonic neutrophils, independently of the host's microbial status (Fig. S1G). In contrast, in steady state, the expression of ICAM-1 and CD146 on the vascular endothelium, both involved in cellular transmigration [23, 24], was influenced by the microbiota: low levels were observed in GF mice, while the expression in OMM¹² + MC² animals was similar to SPF mice (Fig. 3C). Although OMM¹² colonization significantly enhanced endothelial ICAM-1 and CD146, expression levels similar to those in SPF mice were only achieved when the OMM¹² consortium was enriched with *E. coli* and *C. amalonaticus* (MC²) (Fig. 3C). Similarly, normal amounts of the mucosal addressin Mad-CAM-1 [25] were only induced after colonization with the OMM¹² + MC² (Fig. 3C). The impact of the microbiota on activation of endothelial cells was also seen by transcriptome- and gene enrichment analysis (Fig. 3A and B). STRING analysis of significantly upregulated genes in SPF mice compared to GF mice revealed gene networks for cell adhesion, angiogenesis, and lymph vessel development in SPF mice (Fig. 3B). RNA-seq and subsequent pathway analysis revealed that 49 genes involved in angiogenesis were upregulated in colonic endothelial cells from SPF mice (Fig. 3B). In support of this data, microarray analysis of colonic endothelial cells from OMM¹² and OMM¹² + MC² mice disclosed the upregulation of genes that are associated with angiogenesis in OMM¹² + MC² mice (Fig. S2A).

Having observed these angiogenic effects, the colonic tissue was investigated after whole-mount staining by 2-photon microscopy. Similar to previous studies [26], we noticed significantly increased branched crypts in the colon of GF mice (Fig. 3F). While OMM¹² bacteria significantly reduced the numbers of bifurcated crypts, fully separated crypts typical for the mature colon [27] were only seen in OMM¹² + MC² animals (Figs. 3F and 2). Importantly, staining of colonic tissue for CD31⁺ blood vessels revealed that reduced crypt bifurcations were accompanied by an increased number of vascular cross connections between crypts (Fig. 3E). In accordance with these observations, the relative abundance of endothelial cells was higher in OMM¹² + MC² and SPF mice (Fig. 3D). Additionally, we also observed colon size reduction and crypt lengthening after OMM¹² and OMM¹² + MC² colonization (Fig. S2 C and D).

Previous studies have shown that permanent or transient colonization with *Bacteroides thetaiotaomicron* or *E. coli*, respectively, increased the microvascular density of the small intestine [28, 29]. Intravital microscopy revealed increased ramification of the villous vascular network in mice harboring the OMM¹² + MC² bacteria similar to SPF animals (Fig. 3G). The microvascular density of OMM¹² mice was slightly increased as compared to GF mice, indicating that bacterial strains present in the OMM¹² consortium have a limited potential to induce angiogenesis in the small intestine. Importantly, OMM¹² + MC² but not OMM¹² consortia triggered ileal VEGFa expression (Fig. S2B).

Collectively, these results indicate that specific commensal bacterial strains activate the intestinal endothelium and promote angiogenesis to enhance leukocyte extravasation in the colon.

Commensal bacteria initiate gene expression of vascular and immune networks in the adult intestine

The cellular and morphological alterations triggered by commensals prompted transcriptome analysis of the whole colon from GF, gnotobiotic, and SPF mice. Animals colonized with OMM¹² or OMM¹² + MC² revealed a considerably overlapping expression profile with SPF mice that was completely distinct from GF animals (Fig. 4E). To visualize differentially expressed transcripts, we first performed a two-group comparison between GF and OMM¹² mice (Fig. 4A–C), which showed upregulated gene networks for innate and adaptive immunity, antimicrobial response, cell adhesion, and epithelial proliferation in OMM¹² mice (Fig. 4C). In contrast, GF mice showed increased transcription of genes involved in the mitotic cell cycle and responses to abiotic stimuli (Fig. 4A). As the addition of MC² to OMM¹² was essential for the clearance of *C. rodentium*, the impact of the two commensals on host gene expression was studied. Gene network analysis between OMM¹² and OMM¹² + MC² indicated that the presence of MC² further amplified the host innate and adaptive immunity but also genes of the antimicrobial response and angiogenesis, e.g., angiopoietin-like 4, the ADM-RAMP2 system, VASH2, Reg3b, and Reg3g (Figs. 4D and S2F).

Interestingly, despite the broad imprinting effects of OMM¹² and MC² bacteria, FISH analysis revealed that this consortium did not invade the colonic epithelium (Fig. S2E).

Together, these findings illustrate that colonization of adult mice with limited numbers of commensal strains was sufficient to induce extensive mucosal reprogramming, comprising the maturation of the intestinal immune and vascular system as well as tissue development.

Contribution of *E. coli* or *C. amalonaticus* to render OMM¹² mice immunocompetent

As the composition and function of microbial communities are shaped by competitive and cooperative interactions among the constituent microbes [30, 31], we next investigated the impact of *E. coli* and/or *C. amalonaticus* on *C. rodentium* elimination in the presence or absence of OMM¹². We noted a significantly reduced pathogen burden after associating OMM¹² mice with *E. coli* in comparison with OMM¹². However, pathogen clearance was not achieved (Fig. 5A). In contrast, OMM¹² + *C. amalonaticus* colonization was sufficient to mediate delayed pathogen clearance after 6 weeks (Fig. 5A), compared to 3 weeks in SPF and OMM¹² + MC² mice (Fig. 1D). As microbial competition for space and resources may have been responsible for these effects, the in vitro potential of *E. coli* and *C. amalonaticus* to compete against *C. rodentium* was studied. While *C. amalonaticus* strongly inhibited the growth of *C. rodentium*, *E. coli* failed to do so comparable to *Enterococcus faecalis* from the OMM¹² and *E. gallinarum* from the MC³ consortium (Fig. 5B). Interestingly, in monocolonized mice, *E. coli*, as previously reported [14], as well as *C. amalonaticus* decreased the *C. rodentium* burden to similar extents, demonstrating that competition mechanisms differ in vitro and in vivo (Figs. 5B and S3A). Colonization of GF mice with both bacteria (MC²) resulted in enhanced pathogen colonization resistance, indicating that both commensals cooperate in vivo (Fig. S3A).

Next, the influence of OMM¹² + *E. coli* and OMM¹² + *C. amalonaticus* on the expression of cell adhesion molecules in endothelial cells was examined. Both groups showed significantly increased ICAM-1 and CD146 expression compared to OMM¹² alone, although *C. amalonaticus* induced a slightly stronger ICAM-1 expression than *E. coli* in the presence of OMM¹² (Fig. 5C). The expression of MadCAM-1, however, was not affected by either commensals (Fig. 5C). Importantly, monocolonization with *E. coli* or *C. amalonaticus* induced similar effects but to a lesser extent (Fig. S3B).

Although in the presence of OMM¹² both bacteria induced strong expression of CD146, a marker for angiogenesis [24], the number of endothelial cells was not increased (Fig. 5D). In agreement with this, enrichment of OMM¹² mice with either *E. coli* or *C. amalonaticus* did not result in crypt maturation and formation of vascular cross connections in the colon, as seen after OMM¹² + MC² colonization (Fig. 5E). On the other hand, monocolonization with *E. coli* or *C. amalonaticus* led to a reduction of bifurcated crypts in ex-GF mice (Fig. S3D), but the relative abundance of endothelial cells remained the same as in GF mice (Fig. S3C). Notably, the relative abundance of endothelial cells increased only once the percentages of bifurcated crypts were approx. 5%, which was only seen in OMM¹² + MC² and SPF mice (Fig. 3F). As the median colon was investigated, we cannot exclude that crypt bifurcations in the proximal or distal colon are also affected by microbial colonization. Conversely, intravital microscopy of the small intestine revealed that monocolonization with *E. coli* or *C. amalonaticus*, or in the presence of OMM¹², increased the density of the capillary network in villi (Figs. 5F and S3E).

Finally, the therapeutic effect of the OMM¹² + MC² consortium in long-term *C. rodentium*-carrier GF mice was examined. GF carriers were first cohoused with OMM¹² mice and subsequently colonized with MC² bacteria (Fig. 5G). Cohousing with OMM¹² mice led to a 200-fold reduction of the fecal pathogen count in the GF carriers, while the OMM¹² cohoused mice became quickly infected with *C. rodentium* (Fig. 5G). Ten days after OMM¹² cohousing, all mice received MC² bacteria, which resulted in a continuous pathogen decrease until its elimination (Fig. 5G). It is noteworthy that both *E. coli* and *C. amalonaticus* stably colonized the animals and were detectable after pathogen clearance (Fig. 5H).

These findings illustrate that the OMM¹² consortium serves as a basis for MC² bacteria to better exert its imprinting effects on the host. Moreover, the cooperation of these 14 bacteria is required for the conversion of *C. rodentium* carriers into responders. In this case, the MC²

(See figure on next page.)

Fig. 3 Commensals activate endothelial cells and promote intestinal angiogenesis. **A** Volcano plot showing fold change of gene expression in colonic endothelial cells of GF and SPF mice. Significant differences in gene expression between the two groups (log₂-fold change ≥ 1 ; p -adj < 0.05) are marked in red. **B** STRING analysis for significantly upregulated transcripts of colonic endothelial cells from SPF mice. **C** Expression of ICAM1⁺, CD146⁺, and MadCAM1⁺ on colonic endothelial cells in indicated mice. **D** Relative abundance (RA) of colonic endothelial cells in the LP of indicated mice. **E** Schematic and microscopic representation of vascular cross connections in the colon. **F** Representative images and quantification of whole-mount staining indicated in mice. Partial vascularized crypts were quantified by insertion of contour surface modules (gray areas). **G** Intravital, multiphoton microscopy of small intestinal blood capillaries after i.v. injection of Qtracker™ 655. Vessel areas were quantified with trace image processing for morphometric measurements within a bounding box (BB). Scale bar: 30 μ m. Results are representative of 4–5 experiments. Shown are representative data of at least two independent experiments with means \pm SD; each symbol represents the individual value for one mouse (C–I). One-way ANOVA was used: **** $p < 0.0001$; ** $p \leq 0.01$; * $p \leq 0.05$; ns, not significant

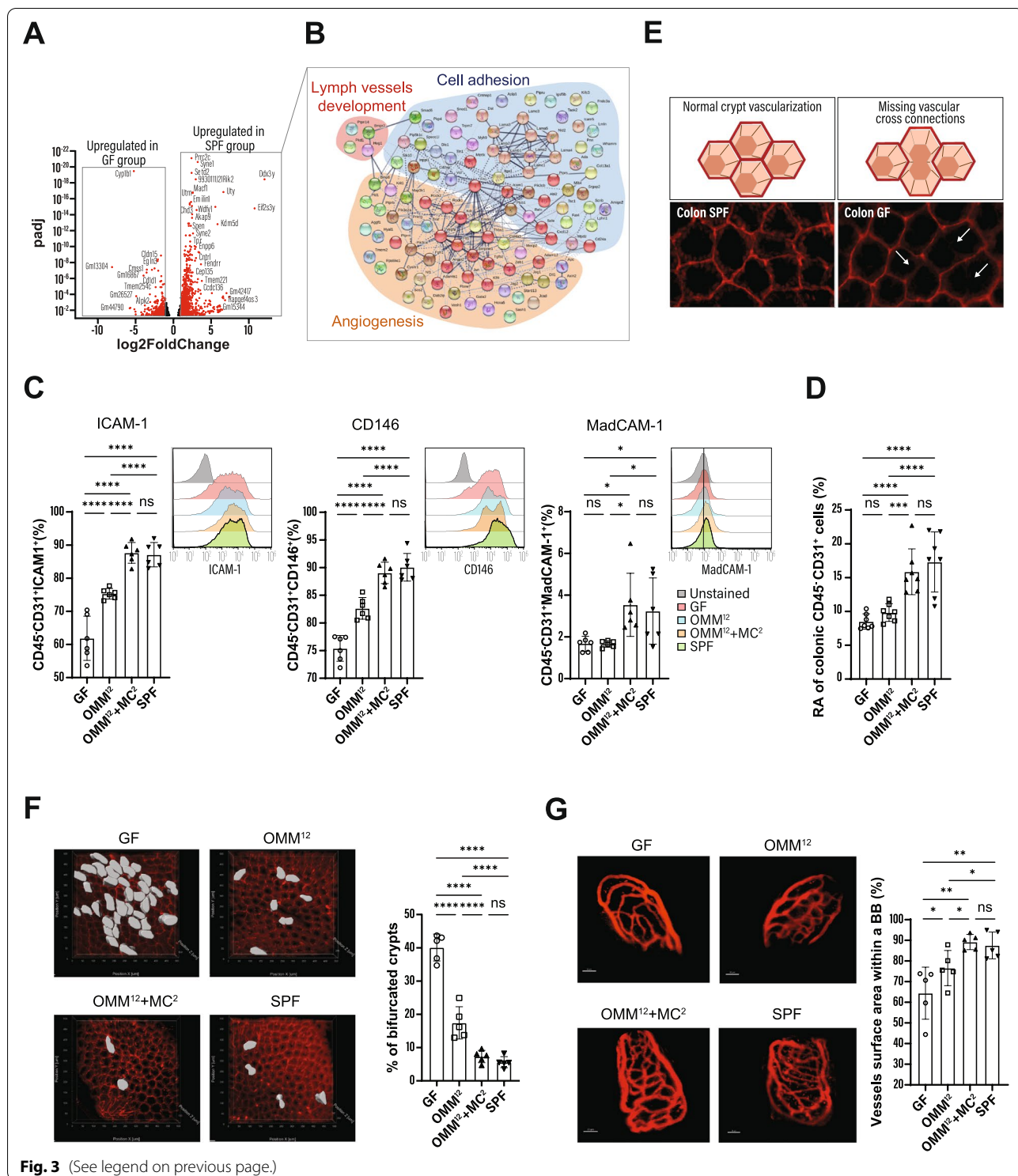


Fig. 3 (See legend on previous page.)

consortium represents two commensals that compensate for partial defects in the microbiota and thus restore immunity via maturation and activation of the gut vascular system.

Discussion

In this study, we show that selected 14 bacterial strains stably colonize the gut of adult GF mice and stimulate morphological and immunological maturation of the

gut. Although the 12 bacteria of the OMM¹² community activated many immune parameters, they were not able to eliminate *C. rodentium*, demonstrating that the presence of two commensals is critical for full immunocompetence. Clearance of *C. rodentium* has been shown to require at least two major steps: first, killing of antibody-coated virulent bacteria by neutrophils in the intestinal lumen, and secondly, metabolic competition and colonization resistance of avirulent bacteria by commensals [14, 19, 20]. Our results revealed that the number and frequencies of blood and colonic LP neutrophils are independent of the microbial status of the host during *C. rodentium* infection, but not those that transmigrate through the colonic epithelium. Here, association of GF animals with OMM¹² + MC² triggered strong migration of neutrophils into the colonic lumen for pathogen engulfment. Thus, trans-endothelial migration of neutrophils into the gut can be modulated by microbial signals. Notably, while OMM¹² colonization induced robust neutrophilic migration during the infection, this was not sufficient to trigger the complete elimination of *C. rodentium*. Since facultative anaerobes are underrepresented in the OMM¹² consortium [16], we propose that MC² bacteria provided bacterial competition which inhibited the expansion of avirulent *C. rodentium* and together with colonic neutrophils led to pathogen clearance. Of note, although *C. rodentium* was avirulent in long-term GF-carrier mice, they were able to spread the pathogen and infect naïve animals, similar to human carriers. It was previously shown that a bicarbonate-rich environment, such as the culture medium DMEM or the gastrointestinal tract, activates *C. rodentium* virulence genes to restore the infectivity of previously avirulent bacteria [32–34].

As composition and function of microbial communities are shaped by competitive and cooperative interactions among the constituent microbes [30, 31], we also dissected the impact of *E. coli* and *C. amalonaticus* during the enteric infection. *C. amalonaticus* in combination with the OMM¹² community led to a substantial delayed but effective clearance of *C. rodentium* infection. This finding supports the observation that SPF mice harboring *C. amalonaticus* show strong colonization resistance against *C. rodentium* infections [18]. In contrast, addition of *E. coli* to OMM¹² mice failed to eliminate the pathogen but showed marginal reduction of the pathogen burden, as previously reported in monocolonized mice

[14]. The fundamental role of the OMM¹² consortium to support MC² bacteria in the progression of intestinal maturation and pathogen clearance is demonstrated in *E. coli* and *C. amalonaticus* monocolonized mice. The only effect shared between all bacterial consortia combinations and OMM¹² + MC² was small intestinal angiogenesis, thus highlighting the complex microbial cooperation between the 14 commensals.

Diapedesis requires the interaction of neutrophil-expressed LFA-1 with ICAM-1, which is expressed on endothelial cells that form the inner cellular lining of blood and lymphatic vessels [22, 35]. Gene analysis of colonic endothelial cells from SPF and OMM¹² + MC² mice revealed that gut commensals promote their activation and proliferation. Remarkably, OMM¹² colonization of GF mice increased the expression of ICAM-1 and CD146 on colonic endothelial cells, but normal levels were only achieved in the presence of MC². Of particular importance was the observation that the OMM¹² + MC² community triggered the development of the villous capillary network in the intestine and induced maturation of the colon via a process called crypt fission [36]. Crypt fission is a developmental process that primarily occurs during the postnatal period and to a much lesser extent in adults [37].

Enrichment of the OMM¹² community with MC² resulted in transcriptional upregulation of several genes expressed in epithelial and/or endothelial cells that protect intestinal stem and Paneth cells from apoptosis and thus contribute to the development of blood vessels, vascular integrity, and homeostasis [38–42]. The Wnt signaling pathway plays a key role in the maintenance and progenitor proliferation of intestinal stem cells, the maturation of Paneth cells, and expression of cryptidins [43, 44]. In line with this, parathyroid hormone-related protein (PTHrP) was upregulated in the colon of OMM¹² + MC², a factor involved in the activation of the Wnt signaling and the regulation of angiogenesis via VEGF expression [45]. Here, VEGF expression was detected in the ileum of OMM¹² + MC² but not OMM¹², demonstrating that cooperation with MC² is essential for triggering angiogenesis in the small intestine and colon.

Finally, an aspect of clinical importance is that the functional interaction between OMM¹² and MC² also works after successive colonization, indicating that pre-existing microbiota can be corrected or complemented.

(See figure on next page.)

Fig. 4 Commensal bacteria initiate gene expression of vascular and immune networks. **A–C** Volcano plot and STRING analysis showing fold change of gene expression in whole colon of GF and OMM¹² mice (**B**). STRING analysis for significantly upregulated transcripts in the colon of GF (**A**) and OMM¹² mice (**C**). **D** Heat map of differentially expressed gene clusters in OMM¹² and OMM¹² + MC² at indicated time points after MC² addition, log₂-fold change ≥ 1; *p*-adj < 0.05. *n* = 4 biological replicates per group. **E** Principal component analysis of colonic gene expression in differently colonized mice. The axes correspond to principal component 1 (x-axis) and 2 (y-axis)

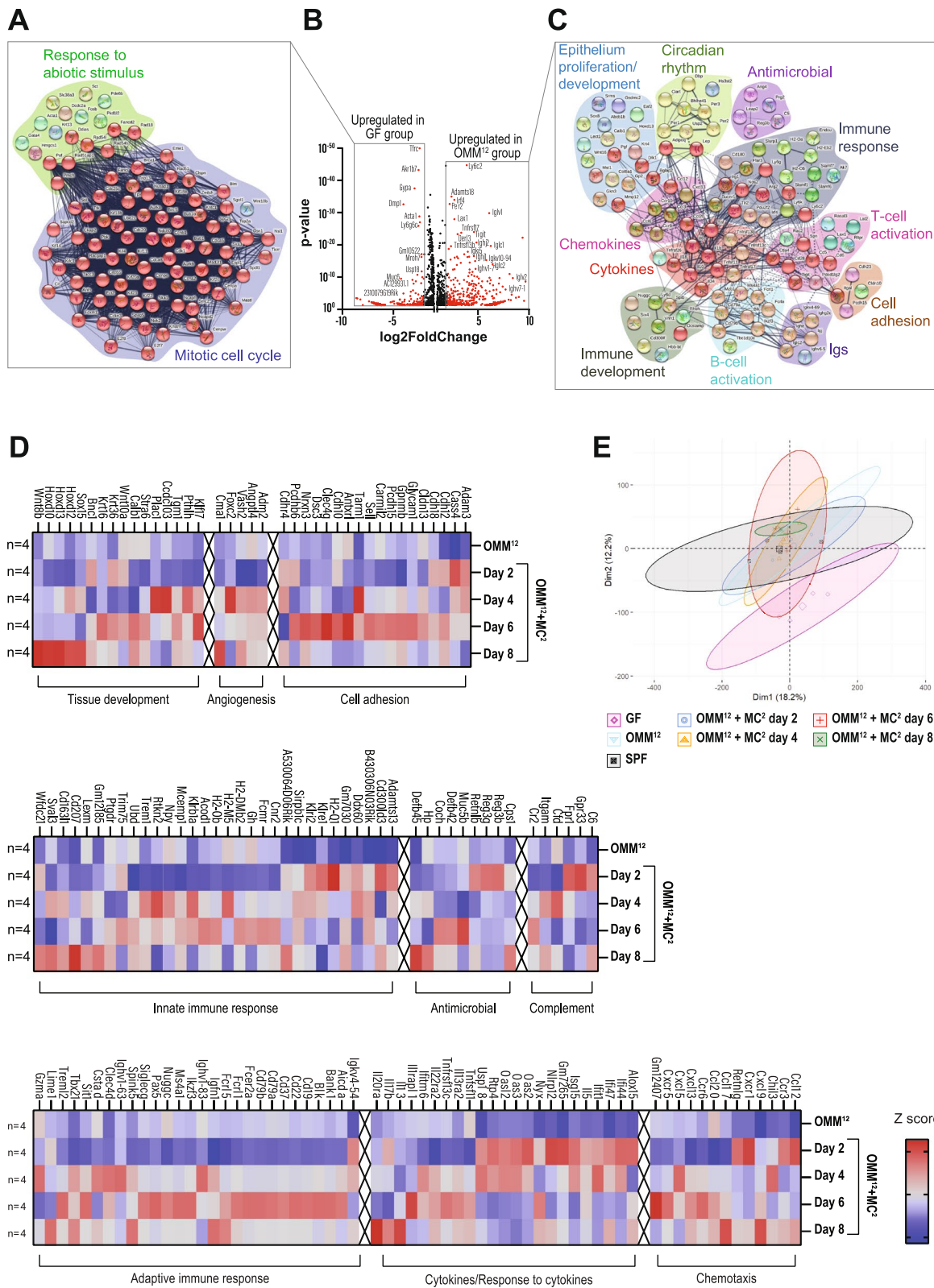


Fig. 4 (See legend on previous page.)

Whether the mechanisms of these microbe-triggered angio- and immunogenic activities involve direct interactions of bacterial ligands such as TLR- or NOD-like receptors [46] and/or indirect ones via metabolites [47, 48] remain to be elucidated, but we are convinced that the observed effects are not limited to the microbial strains used in this study. Although the understanding of commensal-induced tissue and immune-development is complex, our findings give new insights into commensal/microbe-triggered host functionalities. This may be of therapeutic use not only for treatment of asymptomatic carriers of enteropathogens [49] but also for providing an adequate immune response against various assaults [50] or for promoting immune-responsiveness in immunotherapy-refractory patients [51, 52].

In summary, selected commensal bacteria are able to reinitiate ontogeny-like gene expression in the adult intestine, inducing morphological and immunological maturation required for the elimination of enteropathogens.

Conclusions

Our findings revealed that colonization of an enteropathogen carrier with a selected bacterial consortium initiated pathogen elimination. Carrier to responder conversion was made possible through microbe-induced maturation and activation of the intestinal vascular and immune system. Different bacterial consortia have been shown to be of therapeutic value with regard to anticancer immunity [53], chronic infections [54, 55], inflammation [56], or the conversion of immunotherapy-refractory patients into responders [57]. Therefore, we believe that the here observed effects are not exclusively limited to the OMM¹² + MC² community. However, integration and stable colonization of specific bacteria into an existing microbiota are essential prerequisites for microbe-based therapies. Still, intensive research is required to determine the molecular mechanisms by which such microbial consortia act.

In summary, selected commensals are able to reinitiate ontogeny-like gene expression in the adult intestine, thus triggering morphological and immunological maturation, both essential for the elimination of enteropathogens.

Material and methods

Mice

All mice were kept in the animal facility of the Biomedical Research Centre of Philipps-University Marburg. WT mice (C57B/6 background) were purchased from the Charles River Laboratory and bred under specific pathogen-free (SPF) conditions in individually ventilated cages (IVC), with 12-h light cycle, standard rodent pellet diet (LasQCdiet Rod18, HiHyg (Altromin)), and water ad libitum. Germ-free (GF) mice harboring the OMM¹² minimal consortium (C57B/6 background) were kindly provided by Dr. M. Basic (Hannover). GF and gnotobiotic mice were bred in sterile isolators with positive pressure differential and filter-top cages (Tecniplast) with autoclaved bedding, food (Altromin 1324 P Forti), and water ad libitum. Sterility in GF mice was checked monthly by culturing feces in thioglycollate medium under aerobic and anaerobic conditions for at least 10 days as well as fecal gram staining. Contamination in gnotobiotic mice was checked by culturing the feces on blood agar plates under aerobic conditions. All handling procedures for GF and gnotobiotic mice were conducted under a laminar flow hood under sterile conditions.

C. rodentium infection

The nalidixic acid (NA)-resistant wild-type *Citrobacter rodentium* strain DBS 100 was a gift from Till Strowig. For inoculation, bacteria were grown in Luria-Bertani (LB) broth, supplemented with NA (50 µg/ mL) overnight with shaking at 37 °C. Mice were orally infected with 0.2 mL of a *C. rodentium*-PBS suspension (10⁹ CFUs/mL). Bacterial titer was quantified in stool samples by performing serial dilutions, plating bacterial suspensions on LB agar containing NA (50 µg/ mL), and incubating plates overnight at 37 °C.

(See figure on next page.)

Fig. 5 Impact of *E. coli* and *C. amalonaticus* on intestinal maturation and colonization resistance. **A** Course of *C. rodentium* infection in indicated mice. **B** In vitro growth inhibition of *C. rodentium* in the presence of indicated bacteria. Data are shown as fold change compared to *C. rodentium* O/N culture control. **C** Expression of ICAM1⁺, CD146⁺, and MadCAM1⁺ on colonic endothelial cells. **D** Relative abundance (RA) of colonic LP CD45⁻ CD31⁺ endothelial cells in colonized mice. **E** Representative quantification of vascularization in stained whole-mount tissues in indicated mice. Partial vascularized crypts were quantified by insertion of contour surface modules (gray areas). **F** Intravital, multiphoton microscopy of small intestinal blood capillaries after i.v. injection of Qtracker™ 655. Vessel areas were quantified with trace image processing to make morphometric measurements within a bounding box (BB). Scale bar: 30 µm. Results are representative of 4–5 experiments. **G** *C. rodentium* carriers were cohoused with OMM¹² on day 22 p.i. All mice were gavaged 10 days later with MC² bacteria. CFUs of *C. rodentium* were determined in feces. **H** Fecal colonies of *E. coli*, *E. faecalis* (from OMM¹²) and *C. amalonaticus* on Columbia blood agar universal plate from mice of experiment (G) after pathogen elimination. Animals were orally infected with (10⁹ CFU/ml) *C. rodentium*. Data shown are mean ± SD of 2–3 independent experiments; each symbol represents the value for one mouse (D–F). Dotted line represents the reference range for OMM¹² + MC² mice (D–F). One-way ANOVA was used: *****p* < 0.0001; ****p* ≤ 0.01; **p* ≤ 0.05; ns, not significant

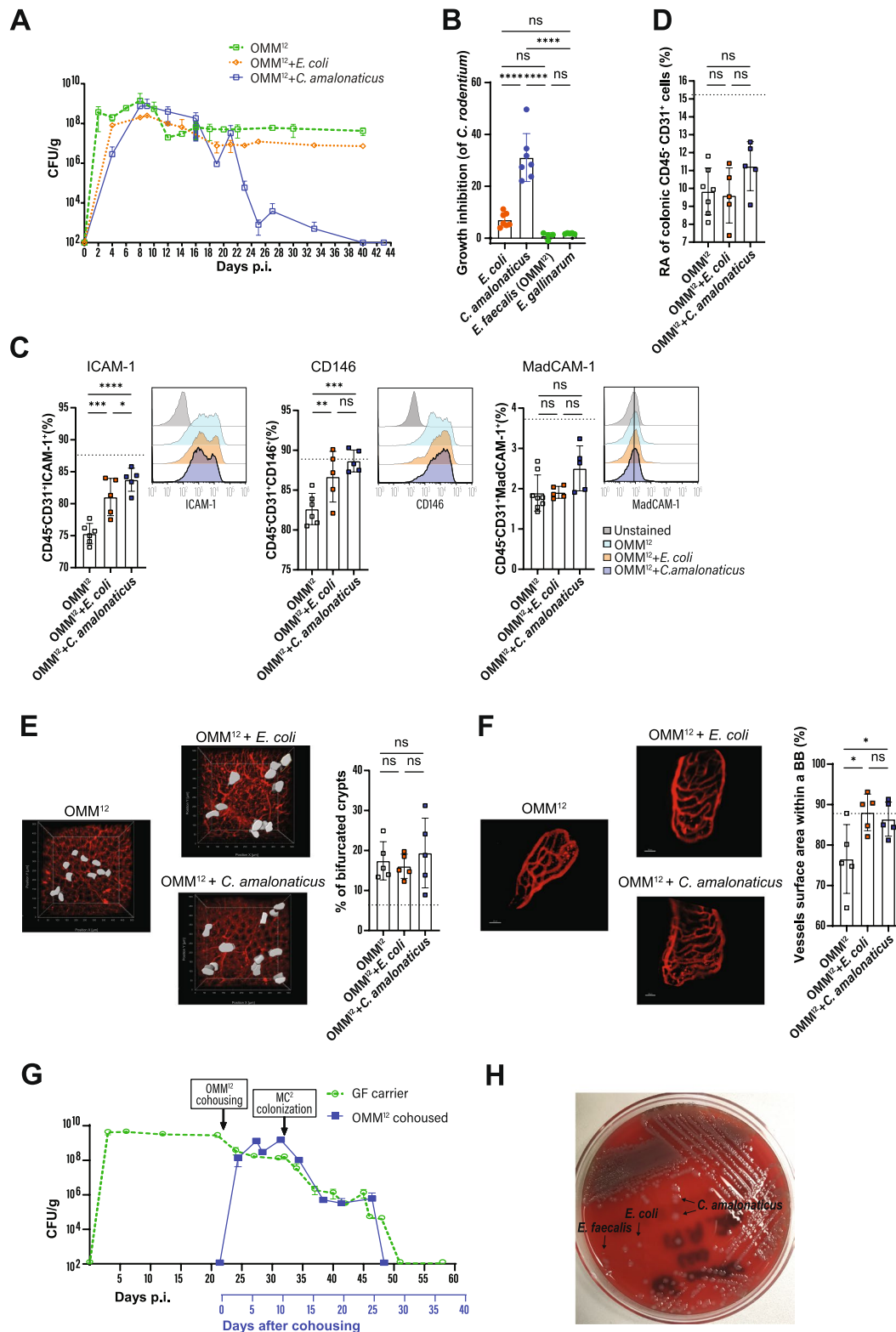


Fig. 5 (See legend on previous page.)

mRNA isolation and qRT-PCR

For total RNA extraction, TRI Reagent (Sigma-Aldrich) was used. RevertAid First Strand cDNA Synthesis Kit (Thermo Scientific) was used to generate complementary DNA (cDNA) according to the manufacturer's instructions. For qRT-PCR, SYBR Green (Applied Biosystems) was applied and the following primer pairs were used:

*ler*Fwd: ACA ACA AGC CCA TAC ATT CAG C

Rev: TGT TAC TTC TTC TTC TGT GTC CTT CA
map Fwd: CCG CTA CAC AAA CTC TTA GAC CAG

Rev: CTT TAC CGC ACT GCT CAT CAAC
espG Fwd: GTG GCG ATT GAT GGG TAA AGAT

Rev: AAA AGC CGT GGA ATG AGA TGAC
espJ Fwd: ATG CTT TTG GTA TCA CTA CGG G

Rev: ATG GGT ATA TGT CAA CAT CCA GTC T
16S Fwd: GGT TGG TGC CTT CGG GAA CTC

Rev: CGC GAG GTC GCT TCT CTT TG

Quantification of cDNA was carried out by normalization to expression of the housekeeping gene *16S* using the $\Delta\Delta C_t$ method.

Application of RB6-8C5 and NIMP-R14 neutrophil-depleting antibodies

RB6-8C5 and NIMP-R14 antibodies were kindly provided by Dr. Friderike Jönsson, from the Institute Pasteur in Paris. They were diluted in PBS and applied i.p. (500 μ g/injection) on the days 5, 8, 11, 14, and 16 p.i. to each mouse.

Fecal microbiota transplant (FMT) of GF mice

Feces from the caecum and colon of SPF mice were homogenized in PBS and given to GF mice infected with *C. rodentium* on day 3 p.i.

Aerobic bacterial suspension from SPF stool samples and bacterial isolation

SPF stool contents from caecum and colon were transferred to an Erlenmeyer flask containing 100 ml LB medium. The suspension was incubated overnight (~16–18 h) at 37 °C. A total of 0.2 ml of the suspension was given to GF mice infected with *C. rodentium* (day 22 p.i.). After pathogen elimination, stool samples from mice that received the aerobic bacteria suspension were homogenized with PBS and streaked onto different agar plates (Columbia-blood agar, chocolate, *Clostridium difficile*, Müeller-Hinton, and Schaedler agar) and incubated under different conditions (aerobic, anaerobic, and CO₂) at 37 °C overnight or until colonies were formed. Colonies with different morphologies were isolated and

streaked onto new plates. The identification of the different isolated bacterial strains was done using matrix-assisted laser desorption ionization time-of-flight mass spectrometry (MALDI-TOF MS).

Sequence analyses of *E. coli* and *C. rodentium*

In short, bacterial genomic DNA was extracted using the PureLink Genomic DNA Mini Kit (Invitrogen) as recommended by the manufacturer. For genome sequencing Illumina short-read sequencing technology and for long-read sequencing, Oxford Nanopore Technology was used. Detailed genome sequencing is given as supplemental information, extended bacteria sequencing.

Briefly, the genome of *Escherichia coli* RSHH22 consists of a circular chromosome of 5,094,340 bp and two extrachromosomal circular sequences designated as plasmid pEC_RSHH22_1 (161,535 bp) and plasmid pEC_RSHH22_2 (4538 bp). The genome harbors 5169 genes in total. We identified eight 5S and seven 16S and 23S rRNA genes. Eighty-nine tRNA genes were detected. The genome of *Citrobacter amalonaticus* RSHH22 consists of a circular chromosome of 4,877,251 bp and one extrachromosomal circular sequence designated as plasmid pCA_RSHH22_1 (110,958 bp). The genome harbors 4808 genes in total. For *Citrobacter amalonaticus* RSHH22, we identified eight 5S and seven 16S and 23S rRNA genes. Eighty-nine tRNA genes were detected. Genome sequence data for *E. coli* RSHH22 and *C. amalonaticus* RSHH22 have been submitted to the NCBI under the accession numbers CP096902-CP096904 and CP096905-CP096906. Potential virulence factor genes and antibiotic resistance genes can be found in supplemental Table 1.

Association of mice with commensal bacteria

A single colony from the isolated bacterial strains was inoculated in 50 ml LB medium and incubated at 150 rpm at 37 °C overnight. The overnight culture was centrifuge (20 min, 4000 rpm at 4 °C). The pellets were resuspended in PBS and mix together as follows:

MC⁵: *L. murinus* (1:4), *E. gallinarum* (1:4), *Paenibacillus* sp. (1:4), *E. coli* (1:8), and *C. amalonaticus* (1:8)

MC³: *L. murinus* (1:3), *E. gallinarum* (1:3), and *Paenibacillus* sp. (1:3)

MC²: *E. coli* (1:1) and *C. amalonaticus* (1:1)

Mice were orally gavage with 0.2 mL of the bacterial-PBS suspension.

Cell isolation techniques

Single-cell suspensions were performed from the intestine by mechanical disruption and passage through filter (Miltenyi Biotec). Lamina propria cells and intraepithelial cells were isolated using the Lamina Propria Dissociation Kit (Miltenyi Biotec) according to manufacturer's instructions. In short, tissues were transferred to pre-heated digestion solution in C tubes (Miltenyi Biotec) and processed by gentleMACS Octo Dissociator (Miltenyi Biotec). The obtained cell suspension was filtered on a 100 μ m cell strainer and washed with MACS buffer. Cells were centrifuged (300 \times g, 4 $^{\circ}$ C, 10 min) and counted using the TC20 automated cell counter (Bio-Rad). Leukocytes were depleted or isolated by incubating the cell suspension with CD45 beads (Miltenyi Biotec). For endothelial activation, the CD45-negative lamina propria cells were further isolated using CD31 beads (Miltenyi Biotec).

Whole blood isolation

Mice were euthanized with isoflurane, and blood was drawn through cardiac puncture. Blood was collected in 2-ml Eppi tubes with HBSS prep supplemented with 80 μ L of heparin solution (25000 I.U./5 ml). Blood was pipetted on top of 3 ml Histopaque 119 (Sigma) in a 15-ml falcon tube to obtain a density gradient. Samples were centrifuged at RT for 5 min at 300 g followed by 20 min at 800 g without break. Interphase containing white blood cells was pipetted into a new 15 falcon tube and wash with FACS buffer. Pellets were treated for erythrocyte lysis with 5 ml NH₄CL solution for 3 min at RT. Cells were centrifuged (300 \times g, 4 $^{\circ}$ C, 10 min) and counted using the TC20 automated cell counter (Bio-Rad).

Cell staining procedures and flow cytometry

Prior to staining for cell surface markers, cell suspension was incubated with FcR Blocking Reagent (Miltenyi) for 10 min at 4 $^{\circ}$ C. Cells were stained by incubation with antibodies diluted in PBS/1%FCS/2 mM EDTA (FACS) buffer for 15 min at 4 $^{\circ}$ C. After further washing with FACS buffer, cells were fixed in 2% formaldehyde for 20 min at 4 $^{\circ}$ C. Flow cytometric analysis was performed after further washing steps, using Attune NxT Flow Cytometer (Thermo Fisher).

For RNA sequencing, CD45⁻CD31⁺ICAM-1⁺CD146⁺ cells were sorted on FACSariaTM III (BD Biosciences).

Whole-mount staining of colonic tissue

Mice were euthanized with isoflurane and perfused with ice-cold PBS containing heparin. Colon was cut longitudinally, and feces were washed out. The tissues were placed in a 12-well plate containing paraformaldehyde (PFA) solution as fixative reagent. After 2 h at 4 $^{\circ}$ C, the

samples were washed 3 times (30 min at 4 $^{\circ}$ C) with PBS with 0.3% Triton X. Tissues were incubated for 2 h at RT in 10% normal goat serum (NGS) containing 0.2% Triton-X. Vessels were stained with Alexa Fluor[®] 594 anti-mouse CD31 antibody (Biolegend) in 2% NGS and incubated for ca. 60 h at 4 $^{\circ}$ C. After antibody incubation, the immunolabeled samples were washed in PBS overnight and transferred into the bracket of the autostainer. The first vial contained a 50% EtOH solution with Aqua ad Iniectionabilia. For adjusting the pH value, 0.1 M NaOH and 0.1 M HCl were used. The samples were placed into an ascending ethanol order, starting from 50 to 70% and two times 100% EtOH, to slowly dehydrate the tissue. Each dehydration step was performed for 4 h. After dehydration, the sample was placed into a glass vessel and incubated with ethyl cinnamate (ECi) (Sigma). After at least 2 h incubation in refractive index (RI) matching agent, the translucent sample was put into a modified view chamber containing ECi and was analyzed using a 2-photon microscope (Olympus FVMPE-RS). For quantification, up to 200 crypts per individual image were examined. Using Imaris surface modules for marking crypts partially surrounded by vascular vessels, the vascularization of crypts was quantified.

Intravital microscopy

Mice were anesthetized by intraperitoneally injection of ketamine (0.1 g/kg BW) and 0.01 g xylazine (0.01 g/kg BW) (injection solution: 10 μ l/g BW). Mice were placed on a preheated plate at 37 $^{\circ}$ C, and the depth of anesthesia was monitored by checking withdrawal reflexes and using the MouseSTAT[®] Jr (Kent Scientific) heart monitor. A small piece of the ileum (~1 cm) was taken, longitudinally open, feces were flushed out, and the tissue was fixed on a preheated metal plate using agarose gel and tissue glue. After preparation of the ileum, mice were injected intravenously with QtrackerTM 655 vascular labels (Invitrogen) to provide real-time vascular contrast. Image acquisition was done using a 2-photon microscope (Olympus FVMPE-RS). Afterwards, mice were euthanized. Quantification was made using Imaris Stitcher and Imaris software (Bitplane) to manually construct surface modules from the fluorescence intensity. The surface area was measured within a surface bounding box area.

Immunohistochemistry VEGF

For immunohistochemistry, heat-induced epitope retrieval was performed with EDTA. Staining was performed on a DAKO autostainer plus. After blocking endogenous peroxidase, sections were incubated for 45 min with mouse monoclonal anti-VEGFA antibody (1:200; Abcam no. ab1316, clone VG-1). Sections were washed and incubated with Dako REAL EnVision HRP Rabbit/Mouse polymer, which

reacts with DAB chromogen, according to the manufacturer's protocol.

Transcriptional profiling

RNA-seq of endothelial cells

For RNA-sequencing of endothelial cells, sorted endothelial cells were resuspended in RLT-buffer containing β -mercaptoethanol. RNA was purified using the RNeasy Plus Micro Kit (Qiagen) according to the manufacturer's instructions. RNA was quantified with a Qubit 2.0 fluorometer (Invitrogen), and the quality was assessed on a Bioanalyzer 2100 (Agilent) using a RNA 6000 Pico chip (Agilent). Samples with an RNA integrity number (RIN) of > 8 were used for library preparation. Barcoded mRNA-seq cDNA libraries were prepared from 20 ng of total RNA using NEBNext[®] Poly(A) mRNA Magnetic Isolation Module and NEBNext[®] Ultra[™] II RNA Library Prep Kit for Illumina[®] according to the manual with a final amplification of 15 PCR cycles. Quantity was assessed using Invitrogen's Qubit HS assay kit, and library size was determined using Agilent's 2100 Bioanalyzer HS DNA assay. Barcoded RNA-Seq libraries were onboard clustered using HiSeq[®] Rapid SR Cluster Kit v2 using 8 pM, and 59 bps were sequenced on the Illumina HiSeq2500 using HiSeq[®] Rapid SBS Kit v2 (59 cycles). The raw output data of the HiSeq was pre-processed according to the Illumina standard protocol. Sequence reads were trimmed for adapter sequences and further processed using Qiagen's software CLC Genomics Workbench (v20 with CLC's default settings for RNA-Seq analysis). Reads were aligned to GRCm38 genome. Total read counts were further processed in R using the DeSeq2 package to compute differential gene expression and adjusted p -values. Gene ontology (GO) analysis and pathway enrichment were performed using PANTHER and AmiGO. Known and predicted interactions for differentially regulated genes (log₂fold change higher than 1 and adjusted p -value lower than 0.05) were derived using the STRING database. The RNA-Seq data were deposited in the Gene Expression Omnibus (GEO) of the National Center for Biotechnology Information and can be accessed with the GEO accession number GSE 180156 (<https://www.ncbi.nlm.nih.gov/geo/query/acc.cgi?acc=GSE180156>).

RNA-seq of whole colon

For whole colon RNA sequencing, colon tissues were preserved directly after dissection in Allprotect Tissue Reagent (Qiagen). Total RNA was isolated using AllPrep DNA/RNA/Protein Mini Kit (Qiagen) according to the manufacturer's instructions. The RNA was treated with RNase-free DNase set (Qiagen cat no.: 79254) and converted to cDNA synthesis technology

and generates Illumina-compatible libraries via PCR amplification (Takara cat no.: 634444). The directionality of the template-switching reaction preserves the strand orientation of the original RNA according to the manufacturer's protocol. Libraries were sequenced for PE100 cycles to a depth of 30 million paired reads using Illumina NovaSeq 6000. Overrepresentation analysis (ORA) and Gene Set Enrichment Analysis (GSEA) were performed for significant differentially expressed protein-coding up- and downregulated genes from RNA-Seq data. Gene Ontology ORA was done using enrichGO method from clusterProfiler. Correlation analysis was performed for normalized counts of all the protein-coding genes from all the samples. The RNA-Seq data were deposited in the Gene Expression Omnibus (GEO) of the National Center for Biotechnology Information and can be accessed with the GEO accession number GSE 181502 (<https://www.ncbi.nlm.nih.gov/geo/query/acc.cgi?acc=GSE181502>).

Microarray analysis

For microarray analysis of endothelial cells, MACS-isolated endothelial cells were resuspended in RLT buffer containing β -mercaptoethanol. RNA was purified using the RNeasy Plus Mini Kit (Qiagen) according to the manufacturer's instructions. RNA quantity and quality were assessed with an Experion StdSens Chip on an Experion[™] Automated Electrophoresis System (Bio-Rad). Microarray experiments were performed as dual-color dye-reversal color-swap hybridizations. Total RNA was labeled with the Low Input Quick-Amp Labeling Kit (Agilent Technologies). In brief, 100 ng total RNA was reverse transcribed and amplified using an oligo-dT-T7 promoter primer and labeled with cyanine 3-CTP and/or cyanine 5-CTP by T7 in vitro transcription. After precipitation, purification, and quantification, 500 ng labeled cRNA of each ratio sample was mixed, fragmented, and hybridized to SurePrint G3 Mouse GE v2 8 × 60 K multipack microarrays (Agilent-074809) according to the supplier's protocol (Agilent Technologies). Scanning of microarrays was performed with 3 μ m resolution and 20-bit image depth using a G2565CA high-resolution laser microarray scanner (Agilent Technologies). Microarray image data were processed with the Image Analysis/Feature Extraction software G2567AA v. A.12.1.1.1 (Agilent Technologies) using default settings and the GE2_1200_Dec17 extraction protocol. The extracted MAGe-ML files were analyzed with Rosetta Resolver, Build 7.2.2 SP1.31 (Rosetta Biosoftware). Color-swap ratio profiles comprising single hybridizations were combined in an error-weighted fashion to create ratio experiments. A 0.5 log₂-fold change expression cutoff for ratio experiments was

applied together with anti-correlation of ratio profiles, rendering the microarray analysis highly significant ($p < 0.05$). In addition, microarray data was analyzed using the R package limma [Ritchie ME, Phipson B, Wu D et al. limma powers differential expression analyses for RNA-sequencing and microarray studies. *Nucleic Acids Res.* 2015;43(7):e47. doi:10.1093/nar/gkv007]. The microarray readout txt files were background corrected, normalized, and controlled for quality [Smyth, G. K., and Speed, T. P. (2003). Normalization of cDNA microarray data. *Methods* 31, 265{273} (version 3.40.6). Within-array normalization was done by locally estimated scatterplot smoothing (Loess), and between-array normalization was done using the Aquantile method. The hybridization control samples were removed, and the gene expression values were averaged for each probe over all replicates of that probe on the microarray, using the avereps function. Microarray data were deposited in the Gene Expression Omnibus (GEO) of the National Center for Biotechnology Information and can be accessed with the GEO accession number GSE 180907 (<https://www.ncbi.nlm.nih.gov/geo/query/acc.cgi?acc=GSE180907>).

STRING analysis for protein-protein interactions (highlighted and labelled) was performed on differentially expressed genes (log₂-fold change > 1; p-adj < 0.05) showing biological processes related to upregulated genes. Line thickness indicates the strength of data supporting the connections between the proteins according to the STRING database. MCL clustering (inflation parameter = 3) was applied to cluster the networks, where every color corresponds to a cluster with similar or associated functions (known and predicted).

Fluorescence in situ hybridization (FISH)

Colonic intestinal tissues containing fecal pellets were fixed overnight with methacarn at room temperature. Tissues were washed in methanol for 30 min, two times in ethanol for 15 min, once in ethanol/xylene (1:1) for 15 min, and two times in xylene for 15 min prior to paraffin embedding.

For FISH analysis, 3–5 μm thin tissue sections were dewaxed and then treated with 50 μl 4% lysozyme solution (45 min, 37 °C) for nucleic acids demasking. After washing, 50 μl hybridization solution (0.9M NaCl, 20 mM Tris-HCL, 0.05% SDS) with the bacterial probe (1:50 Eub338 FITC-GCT GCC TCC CGT AGG AGT) was added and incubated for 3 h at 50 °C. Slides were washed several times at 37 °C and were dried at RT before mounted with ProLong™ Gold Antifade Mountant with DAPI (Thermo Fisher Scientific) following manufacturer's instructions. The samples were documented at a Leica DM5500 wide-field microscope (Leica) and analyzed with Imaris software (Bitplane).

In vitro bacterial competition assay

Bacterial competition assay was performed as previously described with a few modifications [58]. In short, a single colony from *C. rodentium* was incubated in 100-LB medium with a single colony of another commensal bacterial strain overnight at 37 °C (150 rpm). Bacterial suspension was centrifuged, and the CFU/ml of *C. rodentium* was quantified using serial dilutions. Growth inhibition was measured as normalized fold changes to *C. rodentium* normal growth in LB medium.

Statistics

The data were analyzed with GraphPad Prism 9. Significance was calculated using tests indicated in the figure legends. Values less than 0.05 were considered statistically significant.

Abbreviations

ACN: Absolute cell number; BB: Bounding box; CFUs: Colony-forming units; EPEC: Enteropathogenic *E. coli*; EHEC: Enterohemorrhagic *E. coli*; GF: Germ-free; MC: Minimal consortium; LP: Lamina propria; OMM¹²: Oligo-Mouse-Microbiota; O/N: Overnight culture; RA: Relative abundance; SPF: Specific pathogen-free.

Supplementary Information

The online version contains supplementary material available at <https://doi.org/10.1186/s40168-022-01353-5>.

Additional file 1: Figure S1. Microbiota determines neutrophil mediated elimination of *C. rodentium*. (A) Fecal CFU in *C. rodentium* infected SPF and GF mice, after fecal microbiota transplant (FMT) from SPF mice. (B) *C. rodentium*-carriers were gavaged on day 22 pi with an overnight (O/N) aerobic culture of feces from SPF animals, CFUs were determined. (C) Fecal CFUs of *C. rodentium* in indicated mice. (D) Kinetic of colonic neutrophils absolute cell numbers (ACN) during the course of *C. rodentium* infection. (E) Neutrophil frequencies in the colonic lamina propria of indicated mice at day 8 and 10 pi. (F) ACN of neutrophils in the blood of indicated mice at day 8 and 10 pi. (G) Frequencies of LFA-1⁺ neutrophils in the blood and colon of *C. rodentium* infected mice. For *C. rodentium* infection: animals were orally infected with (10⁹ CFU/ml) *C. rodentium*. Data shown are means ±SD and representative of at least two independent experiments, each symbol represents the individual value for one mouse (G-I). One-way ANOVA was used: **** $p < 0.0001$; ** $p \leq 0.01$; * $p \leq 0.05$; ns, not significant. **Figure S2.** Commensal triggered gene expression and macroscopic changes of the colon. (A) Volcano plot showing fold-change of gene expression in colonic endothelial cells of OMM¹² and OMM¹²+MC² (log₂-fold change ≥ 1; p-adj < 0.05). STRING analysis for significantly upregulated transcripts in colonic endothelial cells of OMM¹² (left) and OMM¹²+MC² (right) mice. (B) Representative immunostaining and quantification of VEGFa expression (brown staining) in the ileum of indicated mice. (C) Macroscopic alterations and colon length in response to the microbiota. (D) Quantification of colonic crypt length in indicated mice, each symbol represents one crypt (n=3). (E) OMM¹²+MC² bacteria were visualized by FISH in medial colon (red, bacteria; blue, DAPI). (F) STRING analysis of differentially expressed genes (log₂-fold change ≥ 1; p-adj < 0.05) in complete colon of OMM¹² after colonisation with MC² (n = 4 replicates per group). For *C. rodentium* infection: animals were orally infected with (10⁹ CFU/ml) *C. rodentium*. Data shown are means ±SD; at least two independent experiments were performed, each symbol represents the individual value for one mouse (A, C-F). One-way ANOVA was used: **** $p < 0.0001$; ** $p \leq 0.01$; * $p \leq 0.05$; ns, not significant. **Figure S3.** Effects of GF mice monocolonization with *E. coli* or *C. amalonaticus*. (A) Fecal *C. rodentium*

CFUs in GF and colonized mice after oral infection with *C. rodentium*. (B) Frequencies of ICAM1⁺, CD146⁺ and MadCAM1⁺ colonic endothelial cells in indicated animals. (C) Relative abundance (RA) of LP-isolated CD45⁺CD31⁺ colonic endothelial cells. (D) Representative images and quantification of whole mount staining in indicated mice. Partial vascularized crypts were quantified by insertion of contour surface modules (gray areas). (E) Intravital, multi-photon microscopy of small intestinal blood capillaries after i.v. injection of Qtracker™ 655. Vessel areas were quantified with trace image processing to make morphometric measurements within a bounding box (BB). Scale bar: 30µm. Results are representative of 4-5 experiments. Data represent mean ±SD of 2-3 independent experiments, each symbol represents the value for one mouse (A, B, D-F). Dotted line represents the reference range for OMM¹² mice (D-G). One-way ANOVA was used: *****p* < 0.0001; ** *p* ≤ 0.01; * *p* ≤ 0.05; ns, not significant.

Figure S4. Gene networks from Fig. 4. STRING analysis for significantly upregulated transcripts in the colon of GF (A) and OMM¹² mice (B).

Additional file 2: Supplemental Table 1. Results of virulence factor and antibiotic resistance gene prediction based on blastp&VFDB and RGI&CARD.

Additional file 3.

Acknowledgements

We thank Anne Hellhund and Waltraud Ackermann for expert technical help and Guido Schemken and his animal caretakers for excellent animal care. Thanks to Prof. Till Strowig for providing us with *C. rodentium*, Friderike Jönsson for the kind supply with monoclonal antibodies, and to Dr. Marijana Basic for the excellent supply of gnotobiotic mice. We thank Dr. Fiona Rodepeter for histological analysis, Prof. Paul Bland and Dr. Johannes Mursell for excellent discussions and critical reading of the manuscript, and Dr. Dennis Das Gupta and Dr. Felix Picard for the always helpful advice, support, and discussions.

Authors' contributions

RR, AZ, US, and AV, designed and planned the study. US and RR, wrote the article. RR, AZ, MP, RJ, and CUK performed in vitro experiments and analyzed the data. RR, AZ, FF, KR, HL, HSE, and ML designed and carried out in vivo experiments. KS, KR, WB, MK, HR, and HJM, conducted transcriptome analysis. TH and JPH performed functional genome analysis of bacterial strains. The authors read and approved the final manuscript.

Funding

Open Access funding enabled and organized by Projekt DEAL. This study was supported by the Jürgen Manchot Stiftung to Rossana Romero and the DFG Priority Programm SPP1656 to Ulrich Steinhoff (STE 776/3-1) and André Bleich (BL 953/5-2) and the von Behring Röntgen Stiftung (66-0008) to Ulrich Steinhoff. Torsten Hain was supported by DFG (KFO 309 Z01, SFB1021 Z02, SFB-TR84 B08) and HMWK LOEWE Research Cluster Diffusible Signals project B3

Availability of data and materials

All the data associated with this study are present in the paper or the supplementary materials.

Declarations

Ethics approval and consent to participate

All animal experiments were performed in agreement with the guidelines of the national animal protection law (Tierschutzgesetz (TierSchG) and animal experiment regulations (Tierschutz-Versuchstierverordnung (TierSchVersV)) and the recommendations of the Federation of European Laboratory Animal Science Association (FELASA). The study was approved by the Regierungspräsidentium Gießen (Germany), under project numbers EX7-2015, Ex9-2019, Ex22-2020, Mr 40/2015, and G49/2020.

Consent for publication

Not applicable.

Competing interests

The authors declare that they have no competing interests.

Author details

¹Institute for Medical Microbiology and Hygiene, Philipps-University Marburg, Marburg, Germany. ²Present Address: Cell Biology Unit, University Medical Center, Johannes Gutenberg University, Mainz, Germany. ³Pfizer GmbH, Berlin, Germany. ⁴Department of Environmental Immunology, Helmholtz Centre for Environmental Research — UFZ, Leipzig, Germany. ⁵Institute of Medical Microbiology, Justus Liebig University Giessen, Giessen, Germany. ⁶Partner Site Giessen-Marburg-Langen, German Center for Infection Research (DZIF), Justus Liebig University Giessen, Giessen, Germany. ⁷Center for Tumor Biology and Immunology, Philipps University Marburg, Marburg, Germany. ⁸Pathology, University Hospital of Giessen and Marburg (UKGM), Marburg, Germany. ⁹Medgenome, Inc., San Mateo, CA, USA. ¹⁰Flow Cytometry Core Facility, Philipps University Marburg, Marburg, Germany. ¹¹Medizinische Klinik und Poliklinik II, Universitätsklinikum Würzburg, Würzburg, Germany. ¹²Institute for Lung Research, Universities of Giessen and Marburg Lung Center (UGMLC), Philipps University Marburg, Marburg, Germany. ¹³Institute for Immunology, University Medical Center Johannes Gutenberg University, Mainz, Germany. ¹⁴Tierexperimentelle Einrichtung, Philipps University of Marburg, Marburg, Germany. ¹⁵Department of Cell Biology and Cell Pathology, Philipps University of Marburg, Marburg, Germany. ¹⁶Department of Immunology, Max Planck Institute for Infection Biology, Berlin, Germany. ¹⁷Biomedical Research Center (BMFZ), Institute for Medical Microbiology and Hygiene, University of Marburg, Hans Meerwein Straße 2, 35043 Marburg, Germany.

Received: 20 October 2021 Accepted: 22 August 2022

Published online: 28 September 2022

References

1. Round JL, Mazmanian SK. The gut microbiota shapes intestinal immune responses during health and disease. *Nat Rev Immunol*. 2009;9:313–23. <https://doi.org/10.1038/nri2515> Nature Publishing Group.
2. Derrien M, Alvarez AS, de Vos WM. The gut microbiota in the first decade of life. *Trends Microbiol*. 2019;27:997–1010. <https://doi.org/10.1016/j.tim.2019.08.001> Elsevier Current Trends.
3. Perez PF, Doré J, Leclerc M, Levenez F, Bényacoub J, Serrant P, et al. Bacterial imprinting of the neonatal immune system: lessons from maternal cells? *Pediatrics*. 2007;119:e724–32. <https://doi.org/10.1542/peds.2006-1649> American Academy of Pediatrics.
4. Al Nabhani Z, Dulauroy S, Marques R, Cousu C, Al Bounny S, Déjardin F, et al. A weaning reaction to microbiota is required for resistance to immunopathologies in the adult. *Immunity*. 2019;50:1276–1288.e5. <https://doi.org/10.1016/j.immuni.2019.02.014> Cell Press.
5. Kennedy EA, King KY, Baldrige MT. Mouse microbiota models: comparing germ-free mice and antibiotics treatment as tools for modifying gut bacteria. *Front Physiol*. 2018;9:1534. <https://doi.org/10.3389/fphys.2018.01534> Frontiers.
6. Crabbé P, Nash D, Bazin H, Eysen H, Heremans J. Immunohistochemical observations on lymphoid tissues from conventional and germ-free mice. *Lab Invest*. 1970;22:448–57 Available from: <https://europepmc.org/article/med/4911977>.
7. El Aidy S, van Baarlen P, Derrien M, Lindenbergh-Kortleve DJ, Hooiveld G, Levenez F, et al. Temporal and spatial interplay of microbiota and intestinal mucosa drive establishment of immune homeostasis in conventionalized mice. *Mucosal Immunol*. 2012;5:567–79. <https://doi.org/10.1038/mi.2012.32> Nature Publishing Group.
8. El Aidy S, Hooiveld G, Tremaroli V, Bäckhed F, Kleerebezem M. The gut microbiota and mucosal homeostasis. *Gut Microbes*. 2013;4:118–24. <https://doi.org/10.4161/gmic.23362> Taylor & Francis.
9. Chisholm RH, Campbell PT, Wu Y, Tong SYC, McVernon J, Geard N. Implications of asymptomatic carriers for infectious disease transmission and control. *R Soc Open Sci*. 2018;5. <https://doi.org/10.1098/rsos.172341> The Royal Society Publishing.
10. Arreaza L, De La Fuente L, Vázquez JA. Antibiotic susceptibility patterns of *Neisseria meningitidis* isolates from patients and asymptomatic carriers. *Antimicrob Agents Chemother*. 2000;44:1705–7. <https://doi.org/10.1128/AAC.44.6.1705-1707.2000>.
11. Gerding DN, Muto CA, Owens RC. Measures to control and prevent *Clostridium difficile* infection. *Clin Infect Dis*. 2008;46:S43–9. <https://doi.org/10.1086/521861> Oxford Academic.

12. Barthold SW, Coleman GL, Jacoby RO, Livstone EM, Jonas AM. Transmissible murine colonic hyperplasia. *Vet Pathol.* 2016;15:223–36 SAGE PublicationsSage CA: Los Angeles.
13. Mundy R, MacDonald TT, Dougan G, Frankel G, Wiles S. *Citrobacter rodentium* of mice and man. *Cell Microbiol.* 2005;7:1697–706 Wiley.
14. Kamada N, Kim YG, Sham HP, Vallance BA, Puente JL, Martens EC, et al. Regulated virulence controls the ability of a pathogen to compete with the gut microbiota. *Science (80-).* 2012;336:1325–9 American Association for the Advancement of Science.
15. Faith JJ, Guruge JL, Charbonneau M, Subramanian S, Seedorf H, Goodman AL, et al. The long-term stability of the human gut microbiota. *Science (80-).* 2013;341. <https://doi.org/10.1126/science.1237439> American Association for the Advancement of Science.
16. Brugiroux S, Beutler M, Pfann C, Garzetti D, Ruscheweyh H-J, Ring D, et al. Genome-guided design of a defined mouse microbiota that confers colonization resistance against *Salmonella enterica* serovar Typhimurium. *Nat Microbiol.* 2016;2:1–12. <https://doi.org/10.1038/nmicrobiol.2016.215> Nature Publishing Group.
17. Bingle LEH, Constantinidou C, Shaw RK, Islam MS, Patel M, Snyder LAS, et al. Microarray analysis of the *Ler* regulon in enteropathogenic and enterohaemorrhagic *Escherichia coli* strains. *PLoS One.* 2014;9:e80160 Public Library of Science.
18. Osbelt L, Thiemann S, SmitN N, Lesker T, Schröter M, Gálvez E, et al. Variations in microbiota composition of laboratory mice influence *Citrobacter rodentium* infection via variable short-chain fatty acid production. *PLoS Pathog.* 2020;16. <https://doi.org/10.1371/journal.ppat.1008448>.
19. Kamada N, Sakamoto K, Seo S, Zeng MY, Kim Y, Cascalho M, et al. Humoral immunity in the gut selectively targets phenotypically virulent attaching-and-effacing bacteria for intraluminal elimination. *Cell Host Microbe.* 2015;17:617–27. <https://doi.org/10.1016/j.chom.2015.04.001>.
20. Collins J, Keeney K, Crepin V, Rathinam V, Fitzgerald K, Finlay B, et al. *Citrobacter rodentium*: infection, inflammation and the microbiota. *Nat Rev Microbiol.* 2014;12:612–23. <https://doi.org/10.1038/nrmicro3315>.
21. Gorina R, Lyck R, Vestweber D, Engelhardt B. β 2 integrin-mediated crawling on endothelial ICAM-1 and ICAM-2 is a prerequisite for transcellular neutrophil diapedesis across the inflamed blood-brain barrier. *J Immunol.* 2014;192:324–37. <https://doi.org/10.4049/jimmunol.1300858>.
22. Smith C, Marlin S, Rothlein R, Toman C, Anderson D. Cooperative interactions of LFA-1 and Mac-1 with intercellular adhesion molecule-1 in facilitating adherence and transendothelial migration of human neutrophils in vitro. *J Clin Invest.* 1989;83:2008–17. <https://doi.org/10.1172/JCI114111>.
23. Bardin N, Blot-Chabaud M, Despoix N, Kebir A, Harhourri K, Arsanto J-P, et al. CD146 and its soluble form regulate monocyte transendothelial migration. *Arterioscler Thromb Vasc Biol.* 2009;29:746–53. <https://doi.org/10.1161/ATVBAHA.108.183251> Lippincott Williams & Wilkins.
24. Leroyer AS, Blin MG, Bachelier R, Bardin N, Blot-Chabaud M, Dignat-George F. CD146 (Cluster of Differentiation 146). *Arterioscler Thromb Vasc Biol.* 2019;39:1026–33. <https://doi.org/10.1161/ATVBAHA.119.312653> Lippincott Williams & Wilkins Hagerstown.
25. Oshima T, Pavlick K, Laroux F, Verma S, Jordan P, Grisham M, et al. Regulation and distribution of MAdCAM-1 in endothelial cells in vitro. *Am J Physiol Cell Physiol.* 2001;281. <https://doi.org/10.1152/ajpcell.2001.281.4.C1096>.
26. McCullogh J, Ratcliffe B, Mandir N, Carr K, Goodlad R. Dietary fibre and intestinal microflora: effects on intestinal morphometry and crypt branching. *Gut.* 1998;42:799–806. <https://doi.org/10.1136/gut.42.6.799>.
27. Dehmer J, Garrison A, Speck K, Dekaney C, Van Landeghem L, Sun X, et al. Expansion of intestinal epithelial stem cells during murine development. *PLoS One.* 2011;6. <https://doi.org/10.1371/journal.pone.0027070>.
28. Stappenbeck T, Hooper L, Gordon J. Developmental regulation of intestinal angiogenesis by indigenous microbes via Paneth cells. *Proc Natl Acad Sci U S A.* 2002;99:15451–5. <https://doi.org/10.1073/pnas.202604299>.
29. Uchimura Y, Fuhrer T, Li H, Lawson M, Zimmermann M, Yilmaz B, et al. Antibodies set boundaries limiting microbial metabolite penetration and the resultant mammalian host response. *Immunity.* 2018;49:545–559.e5. <https://doi.org/10.1016/j.immuni.2018.08.004>.
30. Figueiredo ART, Kramer J. Cooperation and conflict within the microbiota and their effects on animal hosts. *Front Ecol Evol.* 2020;0:132. <https://doi.org/10.3389/fevo.2020.00132> Frontiers.
31. West S, Griffin A, Gardner A, Diggle S. Social evolution theory for microorganisms. *Nat Rev Microbiol.* 2006;4:597–607. <https://doi.org/10.1038/nrmicro1461>.
32. Abe H, Tatsuno I, Tobe T, Okutani A, Sasakawa C. Bicarbonate ion stimulates the expression of locus of enterocyte effacement-encoded genes in enterohemorrhagic *Escherichia coli* O157:H7. *Infect Immun.* 2002;70:3500–9. <https://doi.org/10.1128/IAI.70.7.3500-3509.2002>.
33. Yang J, Hart E, Tauschek M, Price GD, Hartland EL, Strugnell RA, et al. Bicarbonate-mediated transcriptional activation of divergent operons by the virulence regulatory protein, RegA, from *Citrobacter rodentium*. *Mol Microbiol.* 2008;68:314–27. <https://doi.org/10.1111/j.1365-2958.2008.06171.x> Wiley.
34. Yang J, Tauschek M, Hart E, Hartland EL, Robins-Browne RM. Virulence regulation in *Citrobacter rodentium*: the art of timing. *J Microbiol Biotechnol.* 2010;3:259–68. <https://doi.org/10.1111/j.1751-7915.2009.00114.x> Wiley & Sons, Ltd.
35. Park S, Hyun Y. Neutrophil extravasation cascade: what can we learn from two-photon intravital imaging? *Immune Netw.* 2016;16:317–21. <https://doi.org/10.4110/in.2016.16.6.317>.
36. Bruens L, Ellenbroek S, van Rheenen J, Snippet H. In vivo imaging reveals existence of crypt fission and fusion in adult mouse intestine. *Gastroenterol.* 2017;153:674–677.e3. <https://doi.org/10.1053/j.gastro.2017.05.019>.
37. Dudhwala Z, Hammond P, Howarth G, Cummins A. Intestinal stem cells promote crypt fission during postnatal growth of the small intestine. *BMJ Open Gastroenterol.* 2020;7. <https://doi.org/10.1136/bmjga-st-2020-000388>.
38. Babapoor-Farrokhran S, Jee K, Puchner B, Hassan SJ, Xin X, Rodrigues M, et al. Angiopoietin-like 4 is a potent angiogenic factor and a novel therapeutic target for patients with proliferative diabetic retinopathy. *Proc Natl Acad Sci U S A.* 2015;112:E3030–9. <https://doi.org/10.1073/pnas.1423765112> National Academy of Sciences.
39. Ochoa-Callejero L, Pozo-Rodríguez A, Martínez-Murillo R, Martínez A. Lack of adrenomedullin in mouse endothelial cells results in defective angiogenesis, enhanced vascular permeability, less metastasis, and more brain damage. *Sci Rep.* 2016;6. <https://doi.org/10.1038/srep33495>.
40. Shibuya T, Watanabe K, Yamashita H, Shimizu K, Miyashita H, Abe M, et al. Isolation and characterization of vasohibin-2 as a homologue of VEGF-inducible endothelium-derived angiogenesis inhibitor vasohibin. *Arterioscler Thromb Vasc Biol.* 2006;26:1051–7. <https://doi.org/10.1161/01.atv.0000216747.66660.26>.
41. Shin J, Seeley R. Reg3 proteins as gut hormones? *Endocrinology.* 2019;160:1506–14. <https://doi.org/10.1210/en.2019-00073>.
42. Zhao D, Kim Y, Jeong S, Greenon J, Chaudhry M, Hoepfing M, et al. Survival signal REG3a prevents crypt apoptosis to control acute gastrointestinal graft-versus-host disease. *J Clin Invest.* 2018;128:4970–9. <https://doi.org/10.1172/jci99261>.
43. Mori-Akiyama Y, van den Born M, van Es J, Hamilton S, Adams H, Zhang J, et al. SOX9 is required for the differentiation of paneth cells in the intestinal epithelium. *Gastroenterology.* 2007;133:539–46. <https://doi.org/10.1053/j.gastro.2007.05.020>.
44. van Es J, Jay P, Gregorieff A, van Gijn M, Jonkheer S, Hatzis P, et al. Wnt signalling induces maturation of Paneth cells in intestinal crypts. *Nat Cell Biol.* 2005;7:381–6. <https://doi.org/10.1038/ncb1240>.
45. Isowa S, Shimo T, Ibaragi S, Kurio N, Okui T, Matsubara K, Hassan NM, Kishimoto K, Sasaki A. PTHrP regulates angiogenesis and bone resorption via VEGF expression. *Anticancer Res.* 2010;30(7):2755–67.
46. Schirbel A, Kessler S, Rieder F, West G, Rebert N, Asosingh K, McDonald C, Fiocchi C. Pro-angiogenic activity of TLRs and NLRs: a novel link between gut microbiota and intestinal angiogenesis. *Gastroenterology.* 2013;144(3):613–623.e9. <https://doi.org/10.1053/j.gastro.2012.11.005>.
47. Amedei A, Morbidelli L. Circulating metabolites originating from gut microbiota control endothelial cell function. *Molecules.* 2019. <https://doi.org/10.3390/molecules24213992> MDPI AG.
48. Potente M, Carmeliet P. The link between angiogenesis and endothelial metabolism. *Annu Rev Physiol.* 2017;79:43–66. <https://doi.org/10.1146/annurev-physiol-021115-105134>.
49. Enserink R, Scholts R, Bruijning-Verhagen P, Duizer E, Vennema H, de Boer R, et al. High detection rates of enteropathogens in asymptomatic children attending day care. *PLoS One.* 2014;9. <https://doi.org/10.1371/journal.pone.0089496>.

50. Eberl G. A new vision of immunity: homeostasis of the superorganism. *Mucosal Immunol.* 2010;3:450–60. <https://doi.org/10.1038/mi.2010.20>.
51. Baruch E, Youngster I, Ben-Betzalel G, Ortenberg R, Lahat A, Katz L, et al. Fecal microbiota transplant promotes response in immunotherapy-refractory melanoma patients. *Science.* 2021;371:602–9. <https://doi.org/10.1126/science.abb5920>.
52. Petrof EO, Gloor GB, Vanner SJ, Weese SJ, Carter D, Daigneault MC, et al. Stool substitute transplant therapy for the eradication of *Clostridium difficile* infection: 'RePOOPulating' the gut. *Microbiome.* 2013;1:1–12 BioMed Central.
53. Tanoue T, Morita S, Plichta DR, Skelly AN, Suda W, Sugiura Y, et al. A defined commensal consortium elicits CD8 T cells and anti-cancer immunity. 2019; *Nat.* 565:600–5. <https://doi.org/10.1038/s41586-019-0878-z> Nature Publishing Group.
54. Caballero S, Kim S, Carter RA, Leiner IM, Sušac B, Miller L, et al. Cooperating commensals restore colonization resistance to vancomycin-resistant *Enterococcus faecium*. *Cell Host Microbe.* 2017;21:592–602.e4. <https://doi.org/10.1016/j.chom.2017.04.002> Elsevier.
55. Pereira FC, Wasmund K, Cobankovic I, Jehmlich N, Herbold CW, Lee KS, et al. Rational design of a microbial consortium of mucosal sugar utilizers reduces *Clostridioides difficile* colonization. *Nat Commun.* 2020;11:1–15. <https://doi.org/10.1038/s41467-020-18928-1> Nature Publishing Group.
56. van der Lelie D, Oka A, Taghavi S, Umeno J, Fan T-J, Merrell KE, et al. Rationally designed bacterial consortia to treat chronic immune-mediated colitis and restore intestinal homeostasis. *Nat Commun.* 2021;12:1–17. <https://doi.org/10.1038/s41467-021-23460-x> Nature Publishing Group.
57. Shaikh FY, Gills JJ, Sears CL. Impact of the microbiome on checkpoint inhibitor treatment in patients with non-small cell lung cancer and melanoma. *EBioMedicine.* 2019;48:642–7. <https://doi.org/10.1016/j.ebiom.2019.08.076> Elsevier.
58. Speare L, Septer A. Coincubation assay for quantifying competitive interactions between *Vibrio fischeri* isolates. *J Vis Exp.* 2019;2019. <https://doi.org/10.3791/59759>.

Publisher's Note

Springer Nature remains neutral with regard to jurisdictional claims in published maps and institutional affiliations.

Ready to submit your research? Choose BMC and benefit from:

- fast, convenient online submission
- thorough peer review by experienced researchers in your field
- rapid publication on acceptance
- support for research data, including large and complex data types
- gold Open Access which fosters wider collaboration and increased citations
- maximum visibility for your research: over 100M website views per year

At BMC, research is always in progress.

Learn more biomedcentral.com/submissions

